Inorganic Chemistry

ARTICLE

pubs.acs.org/IC

Water Exchange of a ProHance MRI Contrast Agent: Isomer-Dependent Free-Energy Landscapes and Mechanisms

Rodolphe Pollet,*[,†] Nisanth N. Nair,[‡] and Dominik Marx[§]

[†]DSM/IRAMIS/SIS2M (CEA-CNRS UMR3299), Commissariat à l'Énergie Atomique, 91191 Gif-sur-Yvette, France

[‡]Department of Chemistry, Indian Institute of Technology Kanpur, Kanpur 208016, India

[§]Lehrstuhl für Theoretische Chemie, Ruhr-Universität Bochum, 44780 Bochum, Germany

Supporting Information

ABSTRACT: The water-exchange reaction in two diastereoisomers of the clinical magnetic resonance imaging contrast agent [Gd(HP-DO3A)(H_2O)] (also known as ProHance) has been studied using ab initio simulations. On the basis of the molecular-level details of the mechanism derived from these simulations in aqueous solution, we unravel the underlying difference in the free energies and mechanisms of water exchange in the two diastereoisomers. These findings reveal the crucial role played by hydrogen-bonding dynamics and thus suggest their appropriate control in tailoring improved gadolinium-based constrast agents.

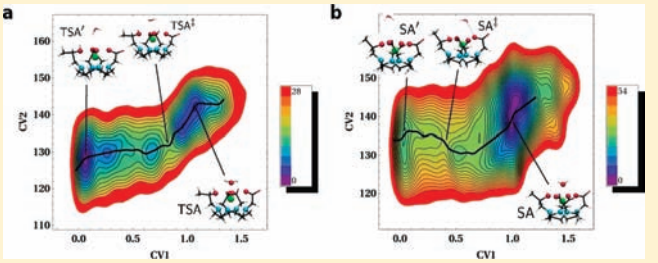

INTRODUCTION

In spite of the low sensitivity of magnetic resonance imaging (MRI) at clinical field strengths, submillimeter spatial resolution can be reached using contrast enhancement. In the presence of paramagnetic contrast agents (CAs), which are often gadolinium(III) chelates, the contrast of so-called T_1-weighted images can be greatly enhanced by the local shortening of the longitudinal relaxation time T_1 of water protons. According to the popular Solomon−Bloembergen−Morgan (SBM) theory,[1,2] this relaxation process is governed by the fluctuating dipolar interactions between the nuclear spin of the protons in the aqueous environment and the large electronic spin localized on Gd^{3+} (where $S = {}^7/_2$). The inner-sphere (IS) contribution to the concentration-normalized T_1 shortening, i.e., the *relaxivity* r_1, is then influenced by a multitude of effects. For low-molecular-weight CAs, the most crucial one is the molecular tumbling rate. To increase the relaxivity, the latter can be slowed down by anchoring the CA onto a macromolecule. Other effects can then be considered for further optimization. One of them is the mean residence time of water in the first coordination sphere τ_M (or equivalently the water-exchange rate $k_{ex} = 1/\tau_M$). For most Gd-based CAs, the time scale of τ_M has to be decreased so that it approaches the optimum value predicted by SBM theory, which is about 10 ns.[3]

In addition to tuning such parameters, stable chelation of Gd^{III} is required to prevent the release of this highly toxic ion in vivo.[4] The chelating ligand molecule considered in this work is 1,4,7-tris(carboxymethyl)-10-(2′-hydroxypropyl)-1,4,7,10-tetraazacyclododecane, abbreviated as HP-DO3A. Therein, four tertiary amines form a basal plane, while three acetates, together with one hydroxypropyl group, form a monocapped plane and, hence, an octadentate ligand overall (Figure 1). The substrate, Gd^{III}, resides between these two twisted planes, thus yielding the overall neutral complex Gd(HP-DO3A). This is also known as gadoteridol or ProHance and is one of the very few clinically approved CAs. Recent medical studies have reported that the injection of ProHance is particularly safe with respect to nephrogenic systemic fibrosis.[5,6]

However, the relaxivity of ProHance is expected to be isomer-dependent (by analogy with DOTAREM), and the average water exchange is slow (i.e., mean residence time τ_M too long) compared to the Gd aqua ion. Two diastereoisomers have been observed in crystals.[7] Isomerization in solution can either proceed via rotation of the carboxylate and hydroxypropyl arms on a 30−50 ms time scale (isomers denoted as Λ or Δ in Figure 1) or via ring inversion on a 10 ms time scale (isomers denoted as $\delta\delta\delta\delta$ or $\lambda\lambda\lambda\lambda$ in Figure 1),[8] which allows thermal equilibrium to be established. If the chiral center on the hydroxypropyl arm of HP-DO3A is ignored, this gives rise to four diastereoisomers, namely, two pairs of enantiomers, $\Lambda(\delta\delta\delta\delta)/\Delta(\lambda\lambda\lambda\lambda)$ and $\Lambda(\lambda\lambda\lambda\lambda)/\Delta(\delta\delta\delta\delta)$. The former isomer adopts the structure of a regular-capped square antiprism (SA),[9] whereas the SA is twisted (TSA) in the case of the latter isomer. On the basis of various experimental obeservations,[10,11] it has been conjectured that the TSA isomer should also be far more efficient than SA for clinical MRI applications using ProHance. Unfortunately, no NMR measurement can actually support these

Received: December 2, 2010
Published: April 26, 2011

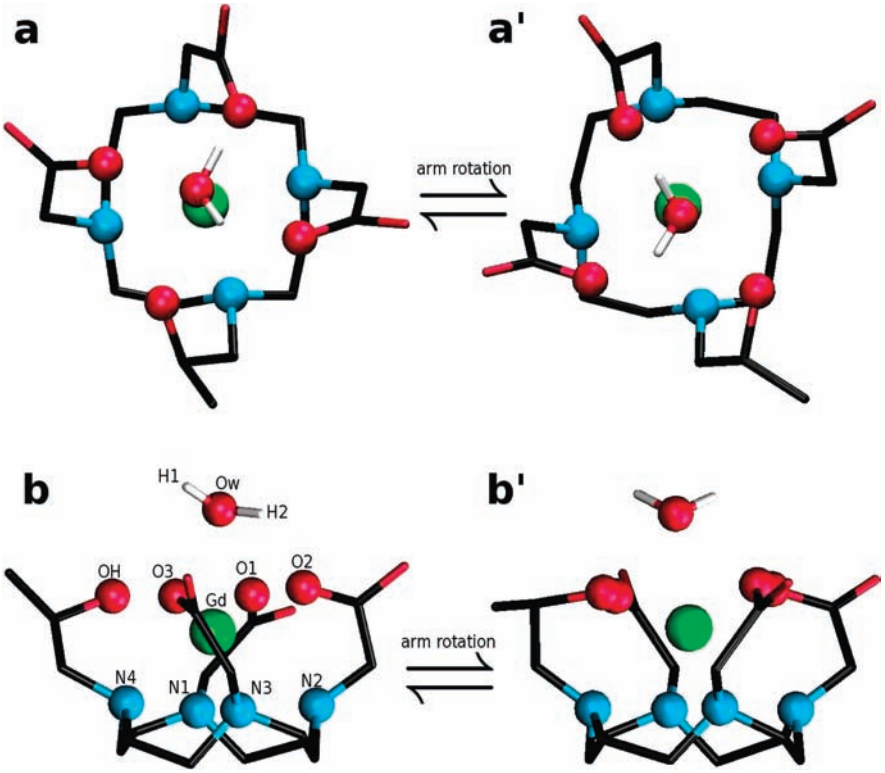

Figure 1. Isomerization between the SA [Λ(δδδδ)] isomer (a, top view; b, side view) and the TSA [Δ(δδδδ)] isomer (a′, top view; b′, side view) of [Gd(HP-DO3A)(H_2O)] using representative structures sampled from equilibrium AIMD simulations in aqueous solution. Only the IS water molecule is shown. Atoms within 3 Å of the Gd cation are highlighted by spheres (Gd, green; H, white; O, red; C, black; N, cyan).

rates because the water exchange in ProHance is so fast as to make only the isomer-averaged and isomer-weighted exchange rates accessible. This situation severely hampers a deeper understanding of the conformational factors that allow one to improve the efficiency of CAs and thus their optimization for clinical use.

Given this situation, computer simulation can complement the experiment by providing mechanistic insight. The starting point is the observation that a dissociative mechanism for IS water exchange has been deduced from large positive values of experimental volumes of activation.[12] Additionally, water exchange in solution is much faster than the conformational dynamics of the chelating arms that interconvert the various isomers.[13] In particular, for [Gd(HP-DO3A)(H_2O)], the mean residence time of the IS water molecule is about 220 ns at 310 K according to ref 14, while the aforementioned isomerizations occur on time scales of tens of milliseconds. On the basis of this hierarchy of time scales, it is possible to compute free-energy barriers to water exchange separately for each isomer of interest. This strategy has been used to elucidate water exchange for both the SA and TSA isomers of the related model complex, $[Gd(DOTA)(H_2O)]^-$, in water using a nonpolarizable force field and rare-event sampling techniques.[15]

However, in view of the 3+ charge of Gd, a real stumbling block is the use of force fields, in particular nonpolarizable ones, to describe IS water exchange in CAs because they neglect the pronounced charge polarization that occurs during water exchange and ligand motion.[16,17] Furthermore, representing the electronic structure of f-block elements such as Gd or Eu using parametrized force fields, which then attempt to accurately describe their interactions both with water molecules and the chelating arms, is a daunting task. A viable alternative to using force fields is performing ab initio molecular dynamics (AIMD),[18] where all interactions are computed "on the fly" from electronic structure theory, thus avoiding any specific parametrization. We have performed AIMD simulation using the Car and Parrinello[19] approach. It has been shown to work favorably for transition-metal and f-block element complexes both in vacuum and in solution.[20−27] However, the exchange reaction of IS water molecules in CAs occurs on the time scale of hundreds of nanoseconds, which is currently far from being accessible to standard AIMD simulation.

Here, we unravel differences in the free-energy landscapes and mechanisms of IS water escape for two ProHance CA isomers in water using AIMD accelerated by the action of a bias time-dependent potential.[18] In particular, we use metadynamics[18,28,29] to escape from free-energy minima and explore free-energy profiles along a high-dimensional reaction coordinate that is based on several hundreds of Cartesian coordinates. As a result of our findings, we propose a novel functionalization strategy that is based on "engineering the hydrogen-bonding network", in order to improve CAs for future clinical use.

METHODS

Electronic Structure Calculations. The electronic structure of Gd(HP-DO3A) in aqueous solution has been described by density functional theory (DFT) using the Perdew−Burke−Ernzerhof functional.[30] Periodic boundary conditions have been applied for an approximately 15.4 Å cubic box that hosts a total of 99 water molecules (i.e., N_w = 99), which corresponds to a water density of approximately 1 g/cm^3. Such a number of solvent molecules provides a proper

dx.doi.org/10.1021/ic102403r |*Inorg. Chem.* 2011, 50, 4791–4797

description of the IS (with 1 or 0 water molecules), the second sphere (i.e., first hydration shell), and the third sphere (i.e., second hydration shell) but leads to truncation of the next water shell. The Kohn−Sham orbitals have been expanded in a plane-wave basis set defined by a cutoff energy of 30 Ry, in conjunction with ultrasoft pseudopotentials[31] for the core electrons. For Gd, a large-core pseudopotential including the 4f electrons in the core has been specifically designed. Its construction rests on the reference (spin-averaged, i.e., nonmagnetic) ground-state electronic configuration of Gd^{2+}, i.e., $[1s^2-4d^{10},4f^7]5s^25p^65d^1$ and incorporates scalar relativistic effects (through Koelling and Harmon's equation[32]) plus a nonlinear core correction[18] with a cutoff radius of 0.90 au; cutoff radii for the s, p, and d channels have all been set to 2.0 au. The performance of this new large-core pseudopopotential has been checked for two microsolvated complexes by comparing to results obtained with a smaller core but also with Gaussian basis set DFT and Moller−Plesset perturbation theory (MP2) calculations (see the Supporting Information). Its accuracy confirms that the seven unpaired 4f electrons play a small role in the prediction of intermolecular geometries and energies. Keeping them in a frozen core means that longer molecular dynamics simulations can be performed due to the closed-shell electronic configuration. All calculations reported herein have been carried out using an in-house-modified version of the CPMD code.[18,33]

Equilibrium Sampling from ab Initio Simulations. The initial configuration of the hydrated chelate has been obtained from crystallographic data,[7] equilibrated with classical molecular dynamics simulations, and eventually relaxed by our short preliminary Car−Parrinello simulation.[22] Two new Car−Parrinello simulations[18,19] have been performed for the SA and TSA isomers to obtain average structural properties and to prepare the subsequent metadynamics simulations. A fictitious electron mass of 700 au and a time step of 6 au, i.e., 0.15 fs, have been used. Nosé−Hoover chain thermostats with a chain length of three have been applied both for ions (with the target temperature set to 300 K) and electrons (with the target fictitious kinetic energy set to 0.032 55 au) to prevent heat transfer between both subsystems. The simulation lengths were 43 and 20 ps for the SA and TSA isomers, respectively.

Exploration of Mechanisms and Computation of Free-Energy Surfaces with Metadynamics. The water-exchange reaction has been investigated by performing ab initio metadynamics simulations.[18,28,29] This method allows one to efficiently cross-pronounce free-energy barriers and enables one to estimate the barrier heights along the minimum free-energy pathway.

For the water-exchange reaction, detachment of the initially coordinated water molecule is described by the change of the coordination number of Gd with respect to *all* water molecules present in the simulation box. This defines the first collective variable

$$\mathrm{CV1} = \sum_{i=1}^{N_w} \frac{1-(d_i/d_0)^p}{1-(d_i/d_0)^{p+q}} \qquad (1)$$

where d_i is the distance between Gd and the ith oxygen, $d_0 = 4.1$ Å, $p = 6$, and $q = 26$. The latter parameters have been carefully chosen after some preliminary tests in order to discriminate clearly all of the expected free-energy minima. Please note that the definition of this collective variable (CV) implies no assumption regarding the reaction mechanism because, from an initial configuration where an IS water molecule is present, CV1 could first decrease from ≈1 to ≈0 (dissociative mechanism) or increase from ≈1 to ≈2 (associative mechanism). In addition, the influence of the opening or closing of the chelate cage, which has previously been shown to be important,[34,35] was probed by a second CV, CV2, which is the average angle ψ of the two bisecting O1−Gd−O3 and O2−Gd−OH angles (see the labels in Figure 1b).

For an efficient sampling and control over the errors in free-energy estimates, we have followed ref 36 for the choice of parameters and protocols for running metadynamics. The height of the Gaussian bias potential used in metadynamics sampling[18] was adapted according to the progression of filling the free-energy wells and varied between $H(t_i) = 0.25$ and 1.0 k_BT. Their dimensionless width was $\delta s(t_i) = 0.05$. For these two CVs, the coupling constants k were 2.0 and 1.5 au, respectively, using a mass parameter of $M = 50$ au in both cases. The metadynamics time step Δt^{meta} was estimated adaptively during the dynamics such that a Gaussian was placed at time t_i once the following condition was fulfilled:

$$|s(t) - s(t_i)| = 3/2\delta s \qquad (2)$$

where $s(t)$ represents auxiliary variables connected to the actual CVs by a harmonic constraint. This condition is necessary to avoid so-called "hill-surfing" artifacts.[37] Moreover, the temperature of the auxiliary variables $\{s_\alpha\}$ was kept within the window of 300 ± 200 K using velocity scaling.

Finally, the free-energy surfaces are reconstructed by the negative sum of biasing potentials.[36] Such free-energy surfaces will enable us to map the minimum-energy pathways connecting various minima and estimate the associated free-energy barriers. It is noted in passing that an absolute free energy is not obtained but only free-energy differences within a simulation. Thus, a comparison between free-energy surfaces computed from two independent simulations cannot be done. In particular, the relative free energies of SA and TSA cannot be computed from the free-energy maps presented here. Our focus here is to only compare the rate of water exchange in the SA and TSA isomers.

Table 1. Selected Average Distances (in Å) from Equilibrium AIMD Simulations for [Gd(HP-DO3A)(H_2O)] in Aqueous Solution for Both SA and TSA Isomers Compared with Available Experimental Results from References 7 and 38[a]

	SA		TSA	
	this work	expt	this work	expt
d(Gd−O_w)	2.62	2.51	2.56	2.50
d(Gd−H_1)	2.89		3.09	
d(Gd−H_2)	3.24		3.10	
d(Gd−HO)	3.14		3.10	
d(Gd−O^P)	0.80	0.75	0.83	0.78
d(Gd−N^P)	1.65	1.61	1.70	1.68
d(cent)	2.44	2.36	2.53	2.46
d(O_w−O^P)	1.82	1.72	1.73	1.76
rmsd	0.09		0.08	

[a] Labels are defined in Figure 1b: HO is the H of the hydroxypropyl group; O^P (N^P) specifies the plane established by O (N) atoms coordinating to Gd, and d(cent) denotes the distance between two centroids formed by N and O atoms coordinating to Gd. The average fluctuation (rmsd) of the metal-to-ligand distances (i.e., involving atoms O1, O2, O3, OH, N1, N2, N3, N4, and O_w) is also reported.

RESULTS AND DISCUSSION

Average Structure of [Gd(HP-DO3A)(H_2O)]. As a first step, a set of important average structural parameters along with their fluctuations as obtained from AIMD simulations have been determined and are compiled in Table 1. The two ProHance isomers SA and TSA have been investigated separately using the computational approach, as detailed in the Methods section. A special word of caution seems appropriate regarding the direct comparison between crystal and computed structures. Indeed, on the one hand, the close proximity of the SA and TSA isomers in the crystallographic study (e.g., the IS water of SA is

dx.doi.org/10.1021/ic102403r |*Inorg. Chem.* 2011, 50, 4791–4797

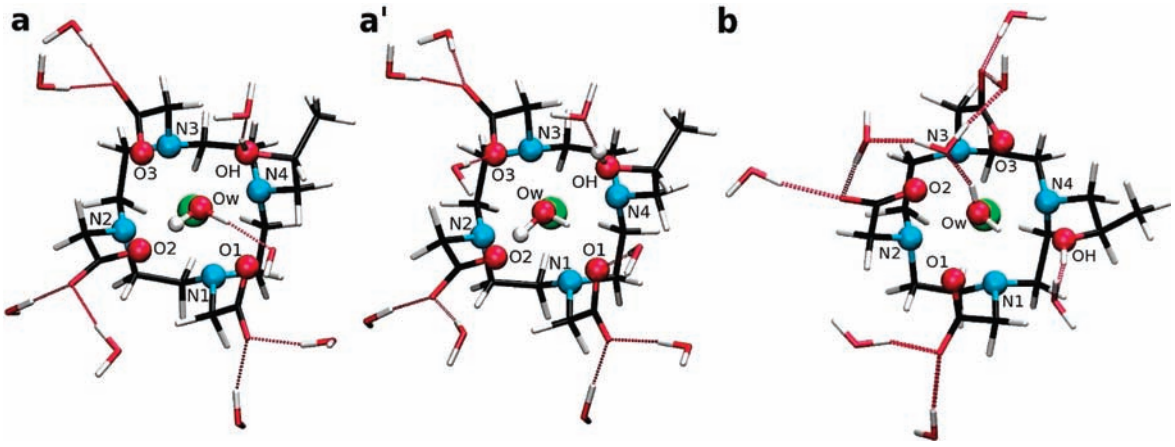

Figure 2. Typical solvation structures around the TSA isomer (a and a′) and SA isomer (b) sampled from equilibrium AIMD trajectories; see Figure 1 for the color code. Only water molecules directly hydrogen-bonded to either the ligand or the IS water molecule are represented. For TSA, the hydrogen bond between the IS and SS water molecules has an occupancy of 42% (a) and the hydrogen bonds between SS water molecules and coordinated carboxylate O atoms O1 and O3 have occupancies of 44% and 56%, respectively (b). For SA, the hydrogen bond between IS and SS water has an occupancy of 65%.

hydrogen-bonded to a carboxylate O atom of TSA) implies a significant interaction between them and, on the other hand, the distributions around the average distances obtained from the simulations are rather broad. With this in mind, it is first reassuring to observe that the most crucial parameters, such as the Gd−O, Gd−N, and Gd−water distances, generally agree to within 5% or better of the crystallographic reference data of the hydrated chelate complex. Importantly, the increases of the distances of Gd to both the O and N planes in the TSA isomer, with respect to the SA isomer, are also correctly reproduced. Our data also directly shed light on a recent proposal put forward to explain the faster water-exchange reaction of the TSA isomer of Gd(DOTA-like) complexes in terms of an increased flexibility compared to the SA isomer.[4] The present data do not support this idea because the fluctuations for both isomers do not differ significantly according to the average root-mean-square deviations (rmsd) of distances reported in Table 1.

The average distance between the paramagnetic Gd cation and the closest protons, i.e., those of the IS water molecule, is of utmost importance for the performance of CAs in MRI applications because the relaxivity, r_1, is proportional to this value to the power of −6, according to SBM theory.[1,2] For [Gd(HP-DO3A)-(H_2O)] in a glassy water/methanol solution, the experimental value for this distance, as determined by two-dimensional pulsed electron−nuclear double resonance (ENDOR) spectroscopy,[39] is 3.1 ± 0.1 Å. This is in excellent agreement with the average distance of Gd to the two protons of the bound IS water molecule found for both isomers in the present simulations (i.e., Gd−H_1 and Gd−H_2 in Table 1; see Figure 1b for labeling). We note in passing that the SA isomer clearly features asymmetric water protons, which is in contrast with the TSA isomer. Furthermore, we find that the calculated distribution functions of Gd−H_1 and Gd−H_2 distances overlap with the corresponding distribution of Gd with respect to the H site of the hydroxypropyl arm. These will therefore share similar hyperfine interaction parameters, which is known from the interpretation of peaks in ENDOR spectra.[39]

Hydrogen-Bonding Networks. We now turn our attention to the topology of the hydrogen-bonding network that connects the tightly bound IS water molecule coordinating the Gd site to bulk via the second-sphere (SS) water molecules, which are directly hydrogen-bonded to IS water or to the ligand. Clearly, the formation and rupture of hydrogen bonds at this interface between the CA and bulk solvent might influence not just the magnitude of the exchange rate but also the mechanism of the water-exchange process. In this work, hydrogen-bond analysis will be based on site occupancies according to the criteria that the donor−acceptor distance is less than 3 Å and that the donor−proton−acceptor angle is more than 160°; hydrogen bonds with occupancies exceeding 50% are termed "strong". Their dynamics (e.g., lifetimes) has not been considered in this work. The solvation shell around [Gd(HP-DO3A)(H_2O)] is known to be highly anisotropic because of the strongly hydrophilic centers close to the acetate and hydroxypropyl arms coordinating Gd and also because of the hydrophobic region on the opposite side of the complex.[22] One particularly strong hydrogen bond can be observed for both isomers between the hydroxyl group and a SS water molecule; see Figure 2 for representative snapshots. In addition, each of the free carboxylate O atoms is usually solvated by, on average, two SS water molecules.

Despite these apparent similarities, both isomers exhibit distinctly different hydrogen-bonding topologies. First, the oxygens O1, O2, and O3 coordinating the Gd site are protected from the solvent in the SA isomer, whereas O1 and O3 are partially solvated in the TSA isomer (compare the representative snapshots in parts a′ and b of Figure 2). Consequently, in the TSA isomer, the SS water molecules solvating carboxylate O atoms can be found in close proximity to the IS water and are therefore also good candidates for forming hydrogen bonds with it; hence, a competition exists between these two types of interactions. Second, the IS water molecule can be both a hydrogen-bond acceptor and a donor, but the importance of these interactions is found to depend strongly on the particular isomer. For the SA isomer, the IS water molecule is a strong hydrogen-bond donor but a weak acceptor. This is quantified by hydrogen-bond occupancies of about 65% for IS water protons H_1 and H_2, compared to only about 32% for the IS water oxygen. In contrast, for the TSA isomer, the hydrogen-bond occupancies of IS water protons and oxygen are about 42% and 0%, respectively. Hence, it is a much weaker hydrogen-bond donor than in SA and

dx.doi.org/10.1021/ic102403r |*Inorg. Chem.* 2011, 50, 4791–4797

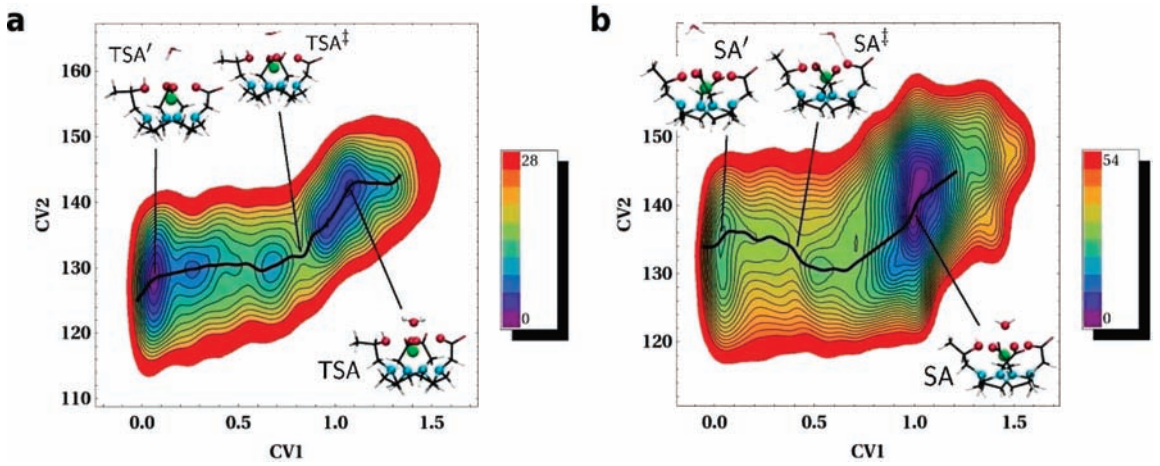

Figure 3. Free-energy surfaces (in units of kJ/mol according to the color scales) for the TSA (a) and SA (b) isomers of [Gd(HP-DO3A)(H_2O)] calculated from ab initio metadynamics simulations. The minimum free-energy paths are indicated by black lines, to which representative snapshots along the reaction coordinate are connected by arrows.

essentially never accepts a hydrogen bond. This can be explained by the presence of nearby water molecules solvating coordinated carboxylate O atoms as mentioned above. Indeed, for the TSA isomer, an SS water molecule can be either a hydrogen-bond acceptor (from the IS water molecule; see Figure 2a) or a hydrogen-bond donor (with respect to, e.g., oxygen O1; see Figure 2a′). In contrast, no such competition appears to exist for the SA isomer and one can therefore assume that the stronger hydrogen bonds between IS and SS molecules in the SA isomer significantly polarize the O−H bond of IS water. This increases the electrostatic interaction between the IS oxygen atom and gadolinium. This could, in turn, result in a higher free-energy barrier for detachment of IS water (in contrast with the TSA isomer), which is the first step in the dissociative mechanism of the water-exchange reaction. However, in view of similar structures at equilibrium, predicting whether one isomer exhibits a lower free-energy barrier than the other one solely based on the different hydrogen-bonding networks is difficult without further knowledge of the reaction pathways.

Free-Energy Landscapes and Water-Exchange Mechanisms. The IS water-exchange reaction is a very slow process, in terms of the time scales accessible to standard AIMD simulations.[18] In order to sample such rare reactive events, the ab initio metadynamics technique[18,28,29] has been used to map the associated free-energy landscapes, which embody the information on free-energy barriers and reaction mechanisms (see the Methods section for details). Crucial to metadynamics is the ability to explore a low-dimensional subspace of the high-dimensional configuration space of the full system, via a set of so-called collective variables (CVs). These CVs are defined in terms of Cartesian coordinates and are chosen such that they contain the true reaction coordinate. On the basis of a series of test simulations, we found two CVs particularly useful: the first (CV1) is the coordination number of the Gd cation to *all* water O atoms available in the system; the second (CV2) is the average of the two O−Gd−O angles involving the four coordinating O atoms (i.e., one from each of the three carboxylate groups and one from the hydroxypropyl arm), which lie diagonally opposite to each other (see the Methods section). It should be stressed that most straightforward CVs, such as the distance between Gd and the O of the bound IS water molecule, fall short in describing the water exchange, and thus a more complex coordinate such as CV2 defined here (which describes the large-amplitude "opening and closing" motion of the entire coordination cage caused by the conformational dynamics of the four chelating arms) turns out to be crucial in this respect. Defining these two CVs implies that, altogether, more than 300 Cartesian coordinates are used in order to describe the reaction coordinate in the (CV1, CV2) subspace. We will use TSA′ and SA′ to denote configurations where no IS water molecule is attached to the Gd site of either the TSA or SA isomer, as appropriate. Thus, the complexes TSA and SA when filled with an IS water molecule are characterized by CV1 $\approx$ 1, whereas the "empty" complexes TSA′ and SA′ correspond to CV1 $\approx$ 0. Crossings of the detachment free-energy barrier from the filled TSA and SA configurations have been observed one and three times, respectively. However, the transition-state region has been visited much more frequently.

Table 2. Selected Average Distances (in Å) for the TSA and SA Isomers of [Gd(HP-DO3A)] in Aqueous Solution from the Two Metadynamics Simulations[a]

	SA	SA′	SA‡	TSA	TSA′	TSA‡
d(Gd−O_w)	2.55			2.60		
d(Gd−H_1)	2.85			3.07		
d(Gd−H_2)	3.18			3.18		
d(Gd−HO)	3.11	3.19	3.16	3.12	3.19	3.13
d(Gd−O^P)	0.79	0.93	0.93	0.84	1.03	0.95
d(Gd−N^P)	1.64	1.56	1.54	1.71	1.55	1.61
d(cent)	2.43	2.49	2.47	2.54	2.58	2.56

[a] The primes denote the isomers where the IS water molecule has been expelled and the double dagger refers to the transition state. Labels are defined in Figure 1b and Table 1.

The free-energy landscapes obtained for water exchange in the TSA and SA isomers feature a rich structure, in the sense of a nonlinear interplay of the two CVs, which both contribute to the reaction coordinate. The Helmholtz free-energy barriers (as obtained from the free-energy pathways drawn on top of the surfaces in Figure 3 and corresponding to IS water loss) can be estimated as approximately 13 and 33 kJ/mol for the TSA and SA isomers, respectively. A free-energy barrier of 37 kJ/mol at 300 K

dx.doi.org/10.1021/ic102403r |*Inorg. Chem.* 2011, 50, 4791–4797

has been reported experimentally[14] for a solution of Gd(HP-DO3A) in water. It should be noted that the solution of Gd(HP-DO3A) contains both SA and TSA isomers, depending on the equilibrium constant of their mutual interconversions. The experimental barrier is much larger than the value determined from the TSA simulation but close to that obtained for the SA isomer. Thus, the corresponding reaction rate deduced from the Eyring–Polanyi equation would actually be about 3 orders of magnitude slower for the SA isomer of ProHance than for the TSA isomer. This underscores the need for active research dedicated to modification of the SA/TSA isomer ratio, that is, in order to develop more efficient CAs by hindering the interconversion of favorable to unfavorable isomers (by, for example, suitably functionalizing the chelating arms and the macrocyclic ring[40]). Important average structural parameters determined for TSA, TSA′, TSA‡, SA, SA′, and SA‡ are complied in Table 2. For both SA and TSA, the average opening/closing angle of the coordination cage, CV2, decreases with progression along the underlying reaction pathway. This corresponds to a closing of the solvation cage formed by the ligands, which drives the detachment of the IS water molecule. This closing is therefore found to be a decisive ingredient for the water-exchange mechanism. In addition, for both isomers, expelling the IS water molecule causes a progressive enlargement of the space enclosed between the two twisted planes, together with a displacement of Gd inside the cage toward the nitrogen plane. Hydrogen-bond occupancies calculated for structures sampled near the TSA free-energy minimum agree with the equilibrium AIMD analysis in that the Gd-coordinated O atoms are partially solvated by SS water molecules and can therefore form fewer hydrogen bonds with the IS water molecule.

These findings make clear the point that comparing the structural parameters for the [Gd(HP-DO3A)(H_2O)] complexes alone does not provide a satisfying explanation for the significant difference in free-energy barrier heights between the isomers. In contrast, our simulations suggest that the free-energy barrier height is dictated by the hydrogen-bond solvation dynamics around the chelate. The picture extracted from the simulation is that there are two competing types of hydrogen bonds involving the SS water molecules: those with the IS water molecule and those with the chelating arms. In the case of the SA isomer, the hydrogen bonds are mostly of the former kind, whereas in TSA, a large number of hydrogen bonds exist between the SS water molecules and the chelate arms (including the coordinating O atoms). Thus, in the SA isomer, the IS water molecule is more firmly kept in the cage by SS water molecules, which increases the free energy to exchange when compared to the TSA isomer. In a nutshell, our simulations suggest that improved CAs could be designed by functionalizing these arms so as to strengthen their hydrogen-bonding interaction with the interfacial SS water molecules.

CONCLUSIONS AND OUTLOOK

Investigations of the water-exchange reaction, being at the heart of understanding and optimizing CAs, have up to now been limited either by the experimental difficulty in directly accessing isomer-specific rate constants or by the predictive power of force-field-based computer simulations. In this work, we take a significant step beyond such simulations by mapping multidimensional free-energy landscapes of the two isomers of ProHance and by unravelling isomer-specific water-exchange mechanisms, using accelerated first-principles simulation techniques.

Although the structural parameters, steric constraints, or flexibility of the ligand could potentially influence the IS water-exchange rates of the SA and TSA isomers of poly(aminocarboxylate) complexes of gadolinium, our ab initio simulations of the ProHance CA stress the role of hydrogen-bond dynamics that couples the first and second solvation spheres. In the case of the TSA isomer, the orientation of its pendant arms favors the formation of hydrogen bonds between SS water molecules and carboxylate O atoms, making the IS water more isolated and, therefore, more labile. For both isomers, water detachment occurs with a closing of the cage formed by the pendant arms of the ligand and causes a displacement of Gd^{3+} toward the N basal plane.

The key conclusion for optimizing CAs is that our results suggest a paradigmatic shift from modifying steric constraints imposed by the chelating arms toward functionalizing the chelating arms, with the aim of enhancing their hydrogen-bonding capabilities (with respect to SS water molecules), i.e., "engineering the hydrogen-bonding network". This could be achieved, for instance, by adding hydroxyl groups, primary amines, phosphonates, or sulfonates in close proximity to the IS water molecule, without necessarily increasing the length of the arms. Transcending the specific case, mapping multidimensional free-energy landscapes using accelerated ab initio simulations holds great promise in improving other CAs such as the PARACEST[40,41] family.

ASSOCIATED CONTENT

Supporting Information. Tables of calculated and energetic data. This material is available free of charge via the Internet at http://pubs.acs.org.

AUTHOR INFORMATION

Corresponding Author
*E-mail: rodolphe.pollet@cea.fr.

ACKNOWLEDGMENT

This work was performed using HPC resources from GENCI-CINES and IDRIS (Grant 2009-072195). It was supported by the EC COST Action D-38 Metal-Based Systems for Molecular Imaging Applications and the European Molecular Imaging Laboratories (EMIL) network. Bochum resources came from Research Department "Interfacial Systems Chemistry" (RD IFSC) and Bovilab@RUB.

REFERENCES

(1) Solomon, I. *Phys. Rev.* **1955**, *99*, 559.
(2) Bloembergen, N.; Morgan, L. O. *J. Chem. Phys.* **1961**, *34*, 842.
(3) Caravan, P.; Ellison, J. J.; McMurry, T. J.; Lauffer, R. B. *Chem. Rev.* **1999**, *99*, 2293.
(4) Hermann, P.; Kotek, J.; Kubicek, V.; Lukes, I. *Dalton Trans.* **2008**, 3027.
(5) Penfield, J. G.; Reilly, R. F. *Nat. Clin. Pract. Nephrol.* **2007**, *3*, 654.
(6) Reilly, R. F. *Clin. J. Am. Soc. Nephrol.* **2008**, *3*, 747.
(7) Kumar, K.; Chang, C. A.; Francesconi, L. C.; Dischino, D. D.; Malley, M. F.; Gougoutas, J. Z.; Tweedle, M. F. *Inorg. Chem.* **1994**, *33*, 3567.
(8) Shukla, R. B. *J. Magn. Reson., Ser. A* **1995**, *113*, 196.
(9) Aime, S.; Botta, M.; Ermondi, G. *Inorg. Chem.* **1992**, *31*, 4291.

(10) Aime, S.; Barge, A.; Botta, M.; Sousa, A. S. D.; Parker, D. *Angew. Chem., Int. Ed.* **1998**, *37*, 2673.
(11) Dunand, F. A.; Aime, S.; Merbach, A. E. *J. Am. Chem. Soc.* **2000**, *122*, 1506.
(12) Helm, L.; Merbach, A. E. *Chem. Rev.* **2005**, *105*, 1923.
(13) Aime, S.; Botta, M.; Fasano, M.; Marques, M. P. M.; Geraldes, C. F. G. C.; Pubanz, D.; Merbach, A. E. *Inorg. Chem.* **1997**, *36*, 2059.
(14) Laurent, S.; Elst, L. V.; Muller, R. N. *Contrast Media Mol. Imaging* **2006**, *1*, 128.
(15) Dimelow, R. J.; Burton, N. A.; Hillier, I. H. *Phys. Chem. Chem. Phys.* **2007**, *9*, 1318.
(16) Floris, F. M.; Tani, A. *J. Chem. Phys.* **2001**, *115*, 4750–4765.
(17) Clavaguéra, C.; Sansot, E.; Calvo, F.; Dognon, J.-P. *J. Phys. Chem. B* **2006**, *110*, 12848.
(18) Marx, D.; Hutter, J. *Ab initio Molecular Dynamics: Basic Theory and Advanced Methods*; Cambridge University Press: Cambridge, U.K., 2009.
(19) Car, R.; Parrinello, M. *Phys. Rev. Lett.* **1985**, *55*, 2471.
(20) Ikeda, T.; Hirata, M.; Kimura, T. *J. Chem. Phys.* **2005**, *122*, 244507.
(21) Pollet, R.; Clavaguéra, C.; Dognon, J.-P. *J. Chem. Phys.* **2006**, *124*, 164103.
(22) Pollet, R.; Marx, D. *J. Chem. Phys.* **2007**, *126*, 181102.
(23) Beret, E. C.; Pappalardo, R. R.; Doltsinis, N. L.; Marx, D.; Marcos, E. S. *ChemPhysChem* **2008**, *9*, 237.
(24) Blumberger, J. *J. Am. Chem. Soc.* **2008**, *130*, 16065.
(25) Beret, E. C.; Pappalardo, R. R.; Marx, D.; Marcos, E. S. *ChemPhysChem* **2009**, *10*, 1044.
(26) Seidel, R.; Faubel, M.; Winter, B.; Blumberger, J. *J. Am. Chem. Soc.* **2009**, *131*, 16127.
(27) Moens, J.; Seidel, R.; Geerlings, P.; Faubel, M.; Winter, B.; Blumberger, J. *J. Phys. Chem. B* **2010**, *114*, 9173.
(28) Laio, A.; Parrinello, M. *Proc. Natl. Acad. Sci. U.S.A.* **2002**, *99*, 12562.
(29) Iannuzzi, M.; Laio, A.; Parrinello, M. *Phys. Rev. Lett.* **2003**, *90*, 238302–1.
(30) Perdew, J. P.; Burke, K.; Ernzerhof, M. *Phys. Rev. Lett.* **1996**, *77*, 3865. *Phys. Rev. Lett.* **1997**, *78*, 1396.
(31) Vanderbilt, D. *Phys. Rev. B* **1990**, *41*, 7892.
(32) Koelling, D. D.; Harmon, B. N. *J. Phys. C: Solid State Phys.* **1977**, *10*, 3107.
(33) Hutter, J. *CPMD Software Package*, see www.cpmd.org.
(34) Lukes, I.; Kotek, J.; Vojtisek, P.; Hermann, P. *Coord. Chem. Rev.* **2001**, *216*, 287.
(35) Yerly, F.; Borel, A.; Helm, L.; Merbach, A. E. *Chem.—Eur. J.* **2003**, *9*, 5468.
(36) Nair, N. N.; Schreiner, E.; Marx, D. *J. Am. Chem. Soc.* **2008**, *130*, 14148.
(37) Ensing, B.; Laio, A.; Parrinello, M.; Klein, M. L. *J. Phys. Chem. B* **2005**, *109*, 6676.
(38) In ref 7, *d*(Gd−O3) and *d*(Gd−O7), labeled *d*(Gd−O2) and *d*(Gd−OH) in the present paper, as well as *d*(Gd−N2) and *d*(Gd−N4) were inverted by mistake in Table 6, while the Cartesian coordinates of Table 4 are correct.
(39) Astashkin, A. V.; Raitsimring, A. M.; Caravan, P. *J. Phys. Chem. A* **2004**, *108*, 1990.
(40) Viswanathan, S.; Kovacs, Z.; Green, K. N.; Ratnakar, S. J.; Sherry, A. D. *Chem. Rev.* **2010**, *110*, 2960.
(41) Woods, M.; Woessner, D. E.; Sherry, A. D. *Chem. Soc. Rev.* **2006**, *35*, 500.